



Influence of ZnO addition and milling process on structure and conductivity of $\text{BaCe}_{0.2}\text{Zr}_{0.7}\text{Y}_{0.1}\text{O}_{3-\delta}$ ceramics

Ana Kaori de Oliveira Ouba*, Adilson Luiz Chinelatto, Edson Cezar Grzebielucka, Kethlinn Ramos, Janaina Semanech Borcezi, Adriana Scoton Antonio Chinelatto

PPGECM - Postgraduate Program in Engineering and Materials Science, Department of Materials Engineering, UEPG – State University of Ponta Grossa, Carlos Cavalcanti Avenue, 4748, 84030-900, Ponta Grossa/PR, Brazil

Received 3 March 2021; Received in revised form 12 July 2021; Accepted 26 August 2021

Abstract

Precursor powders for $\text{BaCe}_{0.2}\text{Zr}_{0.7}\text{Y}_{0.1}\text{O}_{3-\delta}$ (BCZY27) ceramics were synthesized by a modified Pechini method and calcined at 900 °C for 12 h. The calcined BCZY27 powders were milled in eccentric and in high energy mill with the addition of 2 and 4 mol% ZnO as sintering aid. The effects of milling and sintering aids on the sinterability and electrical conductivity were studied. The linear shrinkage in thermomechanical analyses started at 1050 °C for the BCZY27 with 4 mol% ZnO processed in eccentric mill. Theoretical density above of 90% TD was obtained for the BCZY27 milled with 4 mol% ZnO and sintered at 1400 °C for 4 h. X-ray diffraction analysis of the BCZY27 ceramics sintered at 1400 °C confirmed the presence of $\text{BaCe}_{0.2}\text{Zr}_{0.7}\text{Y}_{0.1}\text{O}_{3-\delta}$ and $\text{Y}_{0.4}\text{Ce}_{0.6}\text{O}_{1.8}$ phases. The incorporation of Zn into perovskite lattice leads to the secondary phase formation. SEM and EDS analyses confirmed the presence of $\text{Y}_{0.4}\text{Ce}_{0.6}\text{O}_{1.8}$ phase. The sintering was assisted by BaO-ZnO eutectic, which was reflected by the increase of activation energy values for grain boundary conduction. The milling processing did not affect the conductivity properties. The obtained BCZY27 dense sample has conductivity of 7.60×10^{-3} S/cm at 500 °C.

Keywords: perovskite, wet-chemical synthesis, electrical conductivity, impedance spectroscopy, fuel cells

I. Introduction

Solid oxide fuel cells (SOFC) are devices that directly convert chemical energy into electrical energy and stand out for their high conversion efficiency, low gas emission and low impact on the greenhouse effect [1]. Fuel cells are made of two porous electrodes, an anode and a cathode, separated by a dense electrolyte. These components are electrically connected to an external circuit [2].

SOFCs are cells consist of solid and stable electrolytes and present the advantage of one of the highest efficiencies in energy production among the fuel cells. The operation at high temperature allows high reaction kinetics and produces co-generation heating [3]. However, it also poses strict demands regarding the choice of materials and might result in stability and reliability problems [4]. The use of ceramic materials that present

protonic conductivity might reduce the operation temperature and minimize such problems [5].

One of the materials that have drawn attention due to its high protonic conductivity is the doped barium cerate (BaCeO_3). However, this material shows low chemical stability in the presence of H_2O . One way of improving its chemical stability and keeping good conductivity of protons is to produce a solid solution with BaCeO_3 and barium zirconate (BaZrO_3), which presents protonic conductivity and is highly stable. Yttrium oxide (Y_2O_3) is used to create oxygen vacancies by charge compensation, with the substitution of the trivalent Y for tetravalent Ce or Zr at B-site of perovskite structure. The solid solution resulting from these two materials, along with oxygen vacancy former such as yttrium oxide, generates a material with good protonic conductivity and chemical stability [6]. A composition with great potential to be used as a proton conductor electrolyte is $\text{BaCe}_{0.2}\text{Zr}_{0.7}\text{Y}_{0.1}\text{O}_{3-\delta}$ (BCZY27). However, its synthesis is highly complex and requires high sintering tempera-

*Corresponding authors: tel: +55 42 3220 3160, e-mail: anaouba@hotmail.com

ture and long time to achieve high densities [5,7].

One route to obtain BCZY27 is the chemical synthesis following the Pechini method, since it allows the production of high purity fine powders. This process results in good chemical homogeneity of its components and good control of the stoichiometry of complex systems, obtaining powders at relatively low temperatures [8].

The BCZY27 powders produced using the Pechini method, even presenting nanometric sizes, require high temperatures and long sintering times to produce high conductivity dense bodies [9]. One of the strategies employed to reduce the sintering temperature is the use of sintering additives based on transition metal oxides. One of the used additives is ZnO, which might result in a reduction of up to 250 °C in the sintering temperature [10–12]. However, even with the use of additives, depending on the processing used to produce the BCZY27 samples, difficulties to obtain dense bodies might occur.

Thus, the objective of this study was to investigate the production of BCZY27 dense bodies, using synthesis based on the Pechini method with ZnO as a sintering additive paired with grinding during the processing.

II. Experimental

2.1. Powder synthesis

BaCe_{0.2}Zr_{0.7}Y_{0.1}O_{3-δ} powder was synthesized by a modified Pechini method, using stoichiometric amounts of Ba(NO₃)₂ (Vetec-99%), ZrOCl₂ · 8 H₂O (Vetec-99.5%), Ce(NO₃)₃ · 6 H₂O (Vetec-99.5%) and Y(NO₃)₃ · 6 H₂O (Aldrich-99.9%) dissolved in distilled water. Next, precursors were mixed with the reagents: citric acid (Dinâmica-99.5%) and ethylene glycol (Vetec-99.5%) in a 5:1 ratio. The mixture was stirred and heated to 110 °C. After drying, the resin was calcined in two steps, at 350 °C for 4 h and at 900 °C for 12 h.

The obtained BCZY27 perovskite powder was milled using two different procedures to break the agglomerates resulting from the calcination and to reduce the particle size. The first milling was carried out in an eccentric ball mill, BP Instrumentec model CB2-T, for 6 h (referred to as “v”) and the other used a high energy mill, type Spex Certiprep model 8000 Mixer/Mill for 1 h (referred to as “s”). During milling, 2 and 4 mol% of ZnO were added as sintering additive (referred to as

2 and 4, respectively). Zirconia balls, isopropyl alcohol and 1 wt.% polyvinyl butyral (Butvar) were used. The polyvinyl butyral acts as a deflocculant during milling and as a binder during compaction of samples.

After milling, the powders were dried and sieved, and then they were uniaxially pressed (Shimadzu AG-I 300KN) at 500 MPa in discs with 6.4 mm diameter. The sintering of the samples was carried out at 1300 and 1400 °C with a soak time of 4 h and 10 °C/min heating rate. To analyse the effect of milling and the effect of sintering aid the samples prepared from the un-milled powder were sintered at 1600 °C for 4 h and the samples prepared from the ground powder in a high energy mill were sintered at 1600 °C for 12 h.

The sample notation is formed by: composition (BCZY27), amount of sintering aid and used milling process, as detailed in Table 1.

2.2. Characterization

To verify the effect of adding the ZnO sintering additive, a thermomechanical analysis (TMA) was carried out from room temperature to 1350 °C, with a 10 °C/min heating rate using equipment from SETSYS Evolution/Setaram Instrumentation.

The apparent porosity, *AP*, (Eq. 1) and apparent density, *AD*, (Eq. 2) of the sintered samples were measured using the immersion method employing the Archimedes principle in distilled water:

$$AP = \frac{m_{wet} - m_{dry}}{m_{wet} - m_{immersion}} \times 100 \quad (1)$$

$$AD = \frac{m_{dry}}{m_{wet} - m_{immersion}} \cdot \rho_{H_2O} \quad (2)$$

where, *m_{wet}* is wet mass of the sample, *m_{dry}* is dry mass of the sample and *m_{immersion}* is the mass of the samples immersed in distilled water for 24 h.

The identification of crystallographic phases was performed using X-ray diffractometer (Shimadzu, model SSX550), with Cu K α radiation $\lambda = 1.5460 \text{ \AA}$ at scan angle of $2\theta = 5\text{--}90^\circ$ and scanning speed $2^\circ/\text{min}$. Pattern for the sample sintered at 1400 °C was refined using the Rietveld method; this analysis was performed with step of 0.02° and counting time of 4 s per step. The software FullProf Suite supported the data interpretation and the refinement process.

Table 1. Sample notation, processing conditions and apparent porosity (*AP*), apparent density (*AD*) and theoretical density (*TD*) of BCZY27 samples

Sample notation	Amount of ZnO	Milling process	Sintering conditions	<i>AP</i> [%]	<i>AD</i> [g/cm ³]	<i>TD</i> [% TD]
BCZY27	-	-	1600 °C/4 h	42.8	3.49	55.3
BCZY27-s	-	high energy	1600 °C/12 h	39.4	3.71	58.8
BCZY27-v	-	eccentric	1300 °C/4 h	46.8	3.21	50.9
BCZY27-2v	2 mol%	eccentric	1300 °C/4 h	34.7	4.00	63.4
BCZY27-4v	4 mol%	eccentric	1300 °C/4 h	5.2	5.57	88.3
BCZY27-4s	4 mol%	high energy	1300 °C/4 h	4.7	5.70	90.4
BCZY27-4v	4 mol%	eccentric	1400 °C/4 h	4.2	5.75	91.2
BCZY27-4s	4 mol%	high energy	1400 °C/4 h	1.0	5.75	91.2

The microstructure and element distribution of the sintered samples were investigated using field emission scanning electron microscopy, in a Mira 3/Tescan microscope equipped with energy dispersive spectrometer (EDS). For these analyses, the fracture and surface were polished and thermally etched at a temperature 50 °C below the sintering temperature.

The electrical conductivity of the samples was measured using impedance spectroscopy in dry and wet synthetic air atmospheres. These analyses were carried out in an Autolab PGSTAT30 potentiostat. The impedance spectra were analysed using the software Zview® by fitting the data to appropriate equivalent circuits in order to resolve the impedance response as bulk, grain-boundary, and electrode contributions. The measurements were performed on pellets, on which platinum electrodes were deposited, in a frequency range between 1 Hz and 1.2 MHz, at temperatures from 200 to 600 °C with 25 °C intervals. The activation energy (E_a) was determined from a fit of the data to the Arrhenius equation:

$$\sigma \cdot T = A \cdot \exp\left(-\frac{E_a}{K \cdot T}\right) \quad (3)$$

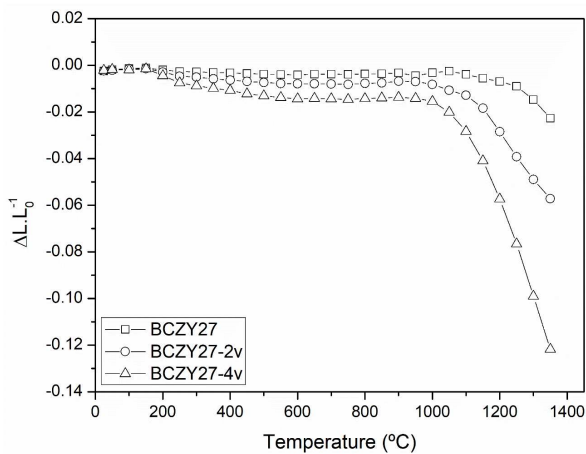


Figure 1. Linear shrinkage of the green BCZY27 pellets prepared from un-ground and ground powders in an eccentric mill with 2 and 4 mol% ZnO additives as function of temperature

where σ is the conductivity, T is temperature and K is the Boltzmann constant.

III. Results and discussion

3.1. Sintering behaviour

Figure 1 shows linear shrinkage of the samples produced with the un-ground BCZY27 powder and powder ground in an eccentric mill with the addition of 2 mol% ZnO (BCZY27-2v) and 4 mol% ZnO (BCZY27-4v). This figure shows that the samples produced with the BCZY27 powders without grinding after synthesis did present a small linear shrinkage, around 2%, indicating low densification up to 1350 °C. This difficulty in initiating shrinking processes during sintering is attributed to the presence of agglomerates. SEM images of the BCZY27 powders after synthesis are shown in Fig. 2. In the sample without milling, Fig. 2a, aggregates were observed. Smaller particles were observed for the milled powders, Figs. 2b and 2c, indicating the efficiency of the grinding in breaking the agglomerates. As it is seen in the literature [13], powders produced by a modified Pechini method generate particles with nanometric or sub-micrometric sizes, these powders are very reactive and lead to the formation of agglomerates during calcination. Thus, during sintering, these pores formed between the agglomerates are difficult to remove and hinder densification.

For the ground powder with 2 mol% ZnO (BCZY27-2v), the shrinkage started at 1100 °C with a total of almost 6%. For the powder with 4 mol% ZnO (BCZY27-4v), the linear shrinkage started at 1050 °C reaching a total of 12%. The curves of the samples with 2 and 4 mol% ZnO submitted to grinding in an eccentric mill have an abrupt shrinkage indicating liquid phase formation. These results showed that the addition of ZnO leads to the increased densification, even at sintering temperatures below 1350 °C. From these results, temperatures of 1300 and 1400 °C were chosen for the sintering of the samples. For comparison purposes, temperature of 1600 °C was also used.

Table 1 presents the apparent porosity, apparent den-

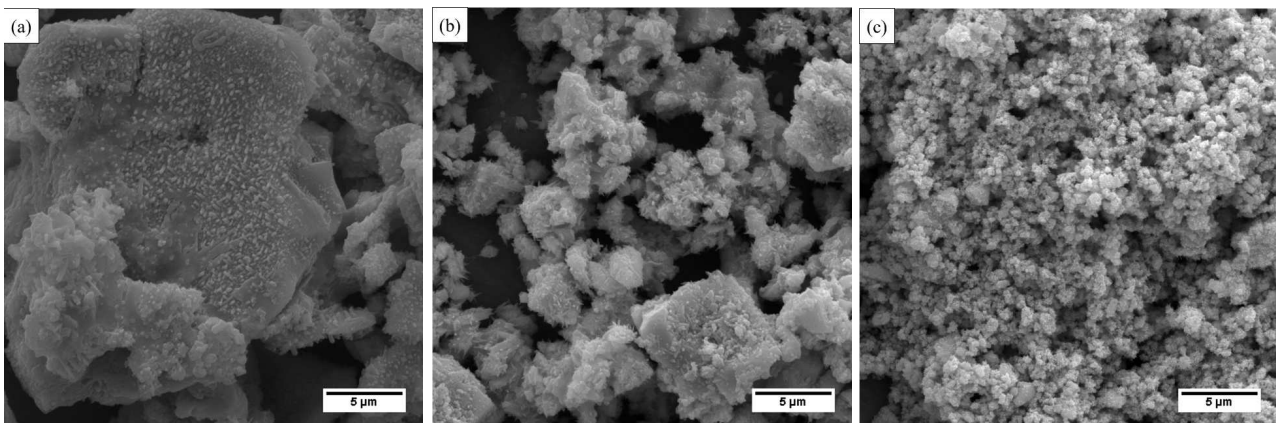


Figure 2. SEM of BCZY27 powders after synthesis: a) without grinding, b) ground in an eccentric mill and c) ground in high energy mill

sity and theoretical density values for the sintered samples. The samples BCZY27 and BCZY27-s sintered at 1600 °C, and the samples BCZY27-v and BCZY27-2v sintered at 1300 °C present extremely high apparent porosity, which resulted in low apparent density. These results show that the breakdown of the agglomerates by grinding was not sufficient to promote improved sintering, even at the temperature of 1600 °C for 12 h. The addition of 2 mol% ZnO accompanied with the powder grinding led to an increase in the density value, even at 1300 °C. However, when 4 mol% ZnO was added, accompanied with the milling in an eccentric mill, a great increase in the density was observed, even when the samples were sintered at 1300 °C. This shows that the amount of sintering aid played an important role in this powder condition. The use of a more energetic grinding (spex mill) led to a greater density increase at 1300 °C. When the sintering temperature was 1400 °C, no difference in the density was found when the two grinding methods were compared.

These results show that the association of milling with the use of ZnO (sintering additive) was efficient to promote the increase in the densification of the material during sintering. The ZnO efficiency as a sintering additive was reported by other authors. Babilo and Haile [10] prepared powders by combustion synthesis and added 4 mol% of ZnO to obtain dense $\text{BaZr}_{0.85}\text{Y}_{0.15}\text{O}_{3-\delta}$ ceramics (>93% TD) at 1300 °C. Tao and Irvine [14] reported a densification of 96% TD with addition of ~3.4 mol% ZnO to $\text{BaZr}_{0.8}\text{Y}_{0.2}\text{O}_{3-\delta}$ obtained by solid state reaction after sintering at 1350 °C. Amsif *et al.* [11] added 4 mol% of zinc nitrate in $\text{BaCe}_{0.9-x}\text{Zr}_x\text{Y}_{0.1}\text{O}_{3-\delta}$ powders prepared by freeze-drying and showed that the samples with $x < 0.5$ sintered at 1200 °C for 10 h reached >95% TD. Reddy and Bauri [15] added Zn in synthesis of $\text{BaCe}_{0.4}\text{Zr}_{0.4}\text{Y}_{0.16}\text{Zn}_{0.04}\text{O}_{3-\delta}$ prepared by gel combustion synthesis and yielded 97% TD at 1300 °C sintering temperature. However, they did not associate the effect of the sintering additive to the milling process.

3.2. Analysis of crystallographic phases

XRD of the BCZY27-4v sintered at 1300 °C for 4 h is shown in Fig. 3. The composition presents a main perovskite (BCZY) phase and the secondary BaCO_3 and ZnO as minority phases. Nasani *et al.* [16] showed that some $\text{BaCe}_{0.8-x}\text{Zr}_x\text{Y}_{0.2}\text{O}_{3-\delta}$ compositions ($x = 0, 0.1, 0.4, 0.6$ and 0.8) prepared using the combustion method also presented BaCO_3 traces, which were eliminated when the calcination temperature reached 1350 °C. The literature also reports the formation of BaCO_3 from $\text{Ba}(\text{OH})_2$ in the $\text{BaCe}_{0.5}\text{Zr}_{0.3}\text{Y}_{0.2}\text{O}_{3-\delta}$ composition that reacts with the CO_2 from the atmosphere [17]. Also, the BaCO_3 and $\text{Ba}(\text{OH})_2$ formation might be the reason for the slow formation of BZY perovskite, resulting in the chemical heterogeneities in the microstructure [18].

The BCZY27-4s sample sintered at 1300 °C presented a diffraction pattern similar to that presented by the BCZY27-4v sample, with the presence of the

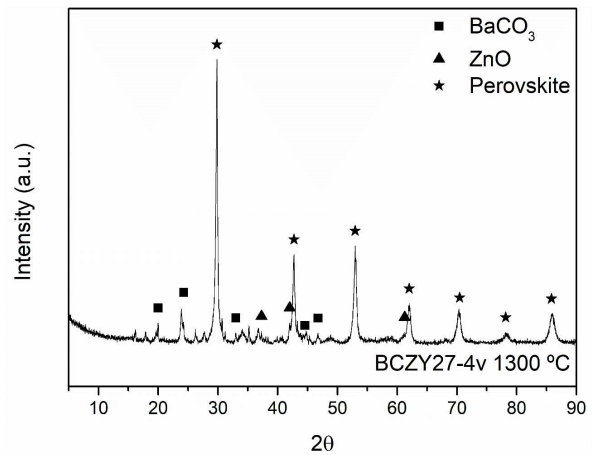


Figure 3. XRD of BCZY27-4v sintered at 1300 °C for 4 h

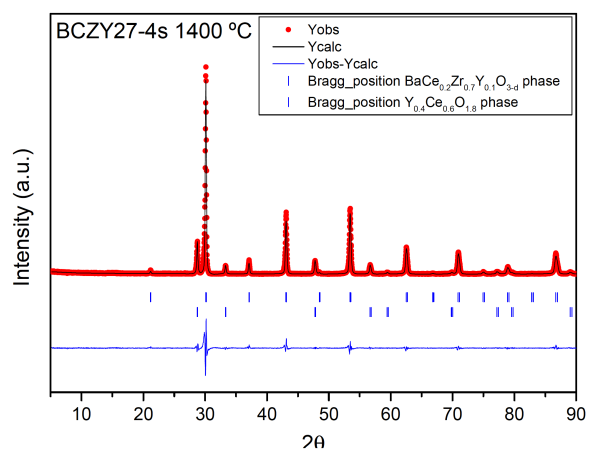


Figure 4. Rietveld refinement of the XRD of BCZY27-4s sintered at 1400 °C for 4 h

BaCO_3 and ZnO phases. Thus, this sample was sintered at 1400 °C in an attempt to form a single phase. Figure 4 shows refined XRD pattern of the BCZY27-4s sintered at 1400 °C, with the refinement parameters $R_p = 12.7\%$, $R_{wp} = 17.2\%$ and $\chi^2 = 3.56$. Stronger XRD peaks correspond to the $\text{BaCe}_{0.2}\text{Zr}_{0.7}\text{Y}_{0.1}\text{O}_{3-\delta}$ phase and small peaks to the $\text{Y}_{0.4}\text{Ce}_{0.6}\text{O}_{1.8}$ phase (Fig. 4), which is a cubic structure of the fluorite type. The $\text{Y}_{0.4}\text{Ce}_{0.6}\text{O}_{1.8}$ phase was formed by the segregation of the elements Ce, Y and O from the BCZY27 phase [12].

Zinc oxide, initially added in concentration of 2 and 4 mol%, is observed in the samples sintered at 1300 °C. When the temperature reached 1400 °C, peaks referring to ZnO were no longer observed by X-ray diffraction. Other authors who did not detect zinc oxide either attributed this to the fact that ZnO could be amorphous, very highly dispersed, or incorporated into the structure [12,19]. It is also believed that ZnO could evaporate during the sintering, or even being undetectable [20].

3.3. Microstructural analysis

The BCZY27 samples were analysed using SEM to observe their microstructure. The BCZY27-4v and BCZY27-4s samples sintered at 1400 °C for 4 h showed

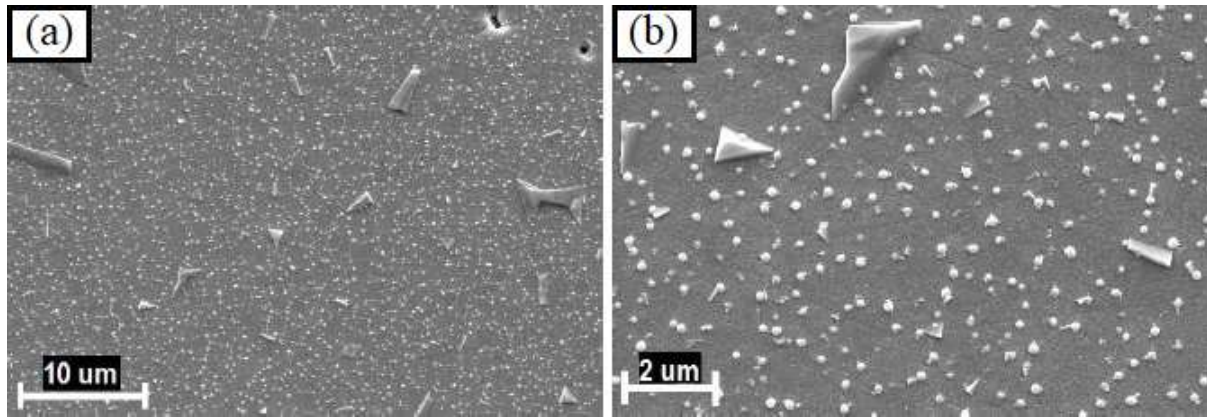


Figure 5. SEM of polished and thermally etched surface of the BCZY27-4v sintered at 1400 °C for 4 h

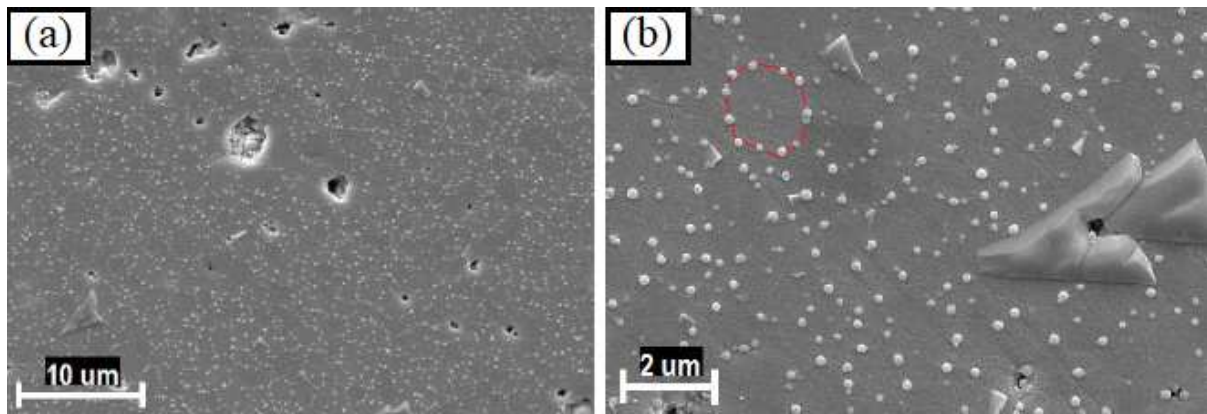


Figure 6. SEM of polished and thermally etched surface of the BCZY27-4s sintered at 1400 °C for 4 h

very similar behaviour, as shown in Figs. 5 and 6. Their microstructures have a low porosity, demonstrating the efficacy of the association of milling and sintering aid. Another finding is the presence of a round-shaped phase, as it can be seen better in higher magnification in Figs. 5b and 6b, which is distributed mainly along the grain boundaries. Such distribution along the grain boundary is more noticeable in the sample BCZY27-4s marked by the red line that was added to Fig. 6b. This phase might have resulted from a liquid phase originating from the formation of the eutectic phase BaZnO_2 at 1099 °C [21]. The appearance of this phase during sintering leads to the BCZY densification and the remaining Zn is later on dissolved in the BCZY phase [10]. This phase is already observed in SEM image of the fractured surface of BCZY27-4s sintered at 1400 °C (Fig. 7). Arrows in Fig. 7 indicate the presence of the round-shape phase during sintering. Uematsu *et al.* [22] reported that addition of BaO as a sintering aid into ZnO led to the rounded grains, suggesting that a liquid phase appears at the grain boundaries. Since this phase was not seen in XRD and the sample was polished and thermally etched, it might have been exuded during additional thermal treatment and thus became more evident.

Another phase with angular shape is also observed in microstructures (Figs. 5 and 6). EDS analysis of the angular phase is shown in Table 2. It can be seen that the quantities of Y and Ce are higher than expected for

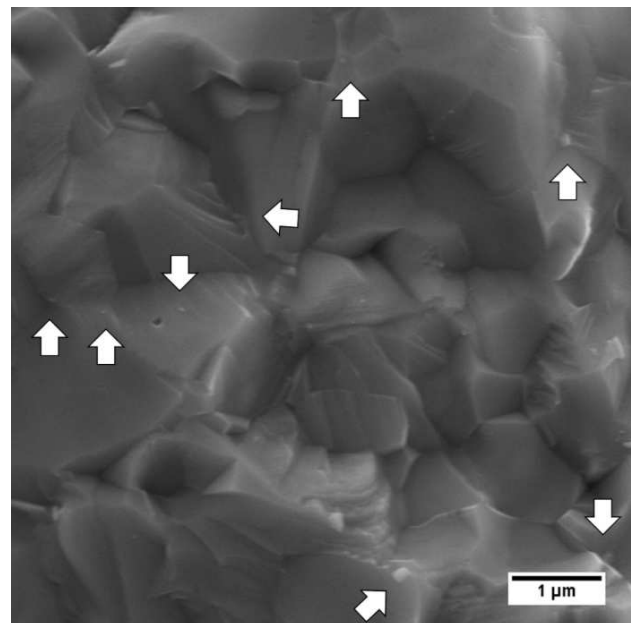


Figure 7. SEM of fracture of surface of the BCZY27-4s sintered at 1400 °C for 4 h

the BCZY27 sample, while the quantities of Zr and Ba are lower than expected for the BCZY27 phase. This phase is like that found by Wendler *et al.* [18], who identified this phase as rich in cerium and yttrium, confirming the XRD of the sample BCZY27-4s sintered at

Table 2. Expected and measured (EDX) elemental composition of Ba, Ce, Zr and Y (EDS microanalysis was carried out at the phases with angular shape)

Element	Expected [at.%]	Measured [at.%]
Ba	50	28.6
Ce	10	21.3
Zr	35	7.3
Y	5	42.8

1400 °C (Fig. 4) where a $Y_{0.4}Ce_{0.6}O_{1.8}$ secondary phase was identified.

Several authors reported the mechanism action of ZnO while adding this sintering additive for better sinterability. Babilo and Haile [10] declared Zn incorporated on the B-site of the perovskite at the grain boundaries, which increased barium vacancy concentration increasing grain boundary mobility, grain growth and densification. Tao and Irvine [14] observed that small amount of Zn^{2+} enters the solid solution occupying the B-site in the perovskite reducing sintering temperature. Wang *et al.* [23] attributed the densification of yttrium-doped $BaCeO_3$ - $BaZrO_3$ to the BaO-ZnO eutectic. Furthermore, they found that the perovskite phase could co-exist with BaO-ZnO, ZnO, Y_2O_3 and Y_2BaZnO_5 . Thus, the addition of 4 mol% of ZnO in BCZY27 by mixing in an eccentric mill or high energy mill results in a liquid phase sintering arising from the BaO-ZnO eutectic, confirmed by SEM images on the fractured surface (Fig. 7) and polished and thermally etched surface (Fig. 6). Nonetheless, $BaCO_3$ and ZnO phases were identified in XRD of BCZY27 sintered at 1300 °C (Fig. 3) and with increasing sintering temperature to 1400 °C, the $BaZnO_2$ formation might be due to the reaction between these reminiscent phases. The excessive ZnO content facilitates the formation of the second phase as it enters the perovskite structure, so $Y_{0.4}Ce_{0.6}O_{1.8}$ phase was formed.

3.4. Electrical conductivity

The samples BCZY27-4v and BCZY27-4s sintered at 1300 and 1400 °C were submitted to impedance spectroscopy in dry synthetic air, to evaluate electrical conductivity. Only the sample BCZY27-4s was also measured in wet synthetic air to evaluate the presence of protonic conductivity.

The Nyquist plot (imaginary impedance (Z'') vs. real impedance (Z')) obtained at 250 °C in dry and wet synthetic air of the sample BCZY27-4s sintered at 1400 °C are shown in Fig. 8. The equivalent circuit used to fit the plots is also presented and it is composed of three resistances (R) connected in series and three constant phase elements (CPE) connected in parallel for each resistance. The added CPE describes the non-ideal capacitance behaviour of depressed semicircles. In the Nyquist plot (Fig. 8) three semicircles are observed. The first semicircle is related to the response of the bulk localized in higher frequencies with capacitance value in the order of 10^{-12} F. The second semicircle is related to the response of the grain boundary, in intermediate frequencies, with capacitance value in the order of 10^{-10} F. The

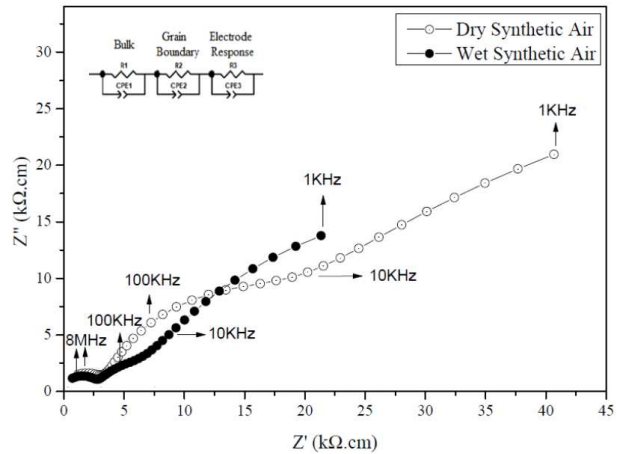


Figure 8. Nyquist impedance plot obtained at 250 °C using wet synthetic air atmosphere for the sample BCZY27-4s sintered at 1400 °C (inset: equivalent circuit)

third semicircle on the right hand site is related to the response of the electrode, in lower frequencies, with capacitance value in the order of 10^{-7} F. The identification of the semicircles that represent the contribution of the bulk, grain boundary and electrode was determined through the capacitance values [24]. Figure 9 shows the Arrhenius plots of total conductivity for the sample BCZY27-4s sintered at 1400 °C for 4 h in dry and wet synthetic air. This figure shows that the measurements carried out in dry synthetic air result in a lower conductivity than those carried out in wet synthetic air. This increase in the conductivity in wet atmosphere confirms the presence of protonic conductivity. In humid atmosphere, materials that present protonic conductivity allow the formation of protonic defects in their structure by the dissociative absorption of water, as shown by the following equation:



where the water from gas phase dissociates into a hydroxide ion and a proton. The hydroxide ion fills an oxide ion vacancy and the proton forms a bond with a lat-

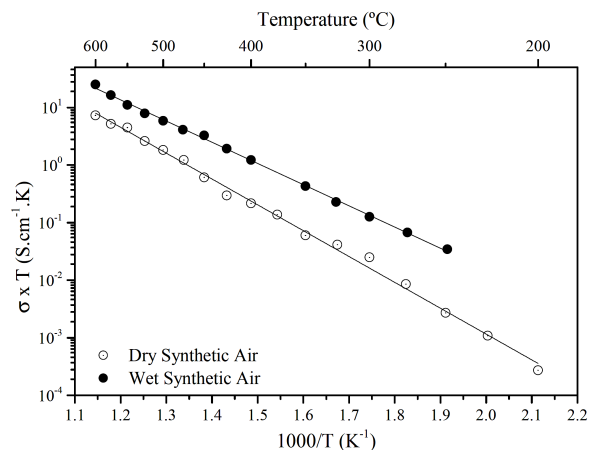


Figure 9. The Arrhenius plots of the total conductivity in dry and wet air for BCZY27-4s sintered at 1400 °C

Table 3. Total conductivity values of BCZY27 samples at 500 °C

Sample	Sintering	Atmosphere	Total conductivity [S/cm]
BCZY27-4v	1300 °C/4 h	dry synthetic air	1.46×10^{-3}
BCZY27-4s	1300 °C/4 h	dry synthetic air	1.11×10^{-3}
BCZY27-4v	1400 °C/4 h	dry synthetic air	2.22×10^{-3}
BCZY27-4s	1400 °C/4 h	dry synthetic air	2.37×10^{-3}
BCZY27-4s	1400 °C/4 h	wet synthetic air	7.60×10^{-3}

tice oxygen [25,26]. The conduction takes place through the Grotthuss mechanism, by hydroxide ion reorientation and transfer of the proton to the adjacent oxygen site [27].

Table 3 shows the comparison of the total conductivity values measured at 500 °C of the samples BCZY27-4v and BCZY27-4s sintered at 1300 and 1400 °C in dry synthetic air and BCZY27-4s sintered at 1400 °C in wet synthetic air. It can be seen that the higher conductivity occurs in humidified atmosphere due to the protons which are the major charge carriers. Moreover, no significant change in the conductivity values was observed as a function of the type of milling used (Table 3), at both sintering temperatures 1300 and 1400 °C. The presence of $Y_{0.4}Ce_{0.6}O_{1.8}$ phase in the sample sintered at 1400 °C did not compromise the total conductivity due to the oxygen ion conduction of this phase [28]. The increase in conductivity with the increase in the sintering temperature is possibly associated with the total porosity reduction, as verified in the apparent density values shown in Table 1.

The influence of sintering aids on the electrical conductivity is very often discussed in the literature. Thus, Jiao *et al.* [29] suggested that the sintering aids segregate at grain boundaries and block proton conduction, revealing a negative effect on the conductivity. Babilo and Haile [10], Reddy and Bauri [15] and Baral [30] explained a reduction in conductivity by attributing it to the defect interactions and associations and the

proton-dopant trapping effect. However, the conductivities measured in this work for the samples BCZY27-4v and BCZY27-4s are close to the values of those reported in the literature without sintering aid. Thus, $BaCe_{0.75}Zr_{0.10}Y_{0.15}O_{3-\delta}$ has total conductivity of 6.37×10^{-3} S/cm at 500 °C in humidified Ar-5% H_2 [31], and $BaCe_{0.3}Zr_{0.55}Y_{0.15}O_{3-\delta}$ reached 3.02×10^{-3} S/cm at 500 °C in humid H_2 [32]. This indicates that despite the addition of sintering aids could be detrimental to electrical conductivity, the amount of 4 mol% ZnO in our case did not produce significant changes in total conductivity.

Figure 10 shows the Arrhenius plots of the samples BCZY27-4s and BCZY27-4v sintered at 1400 °C for 4 h in dry synthetic air. It can be seen that there is no significant variation in bulk, grain boundary and total conductivity values as a function of the type of milling used. What is observed for the samples BCZY27-4s and BCZY27-4v is higher bulk conductivity than grain boundary conductivity. Thus, the total conductivity is limited by the grain boundary conductivity values. Ricote *et al.* [33] observed that the resistivity is in fact higher for the grain boundaries than for the grains and that the zirconate grain boundaries are more resistive than the barium cerate grain boundaries.

Table 4 shows activation energy values for the bulk, grain boundaries and total conductivities of the samples BCZY27-4s and BCZY27-4v sintered at 1400 °C. The activation energy for conduction calculated from

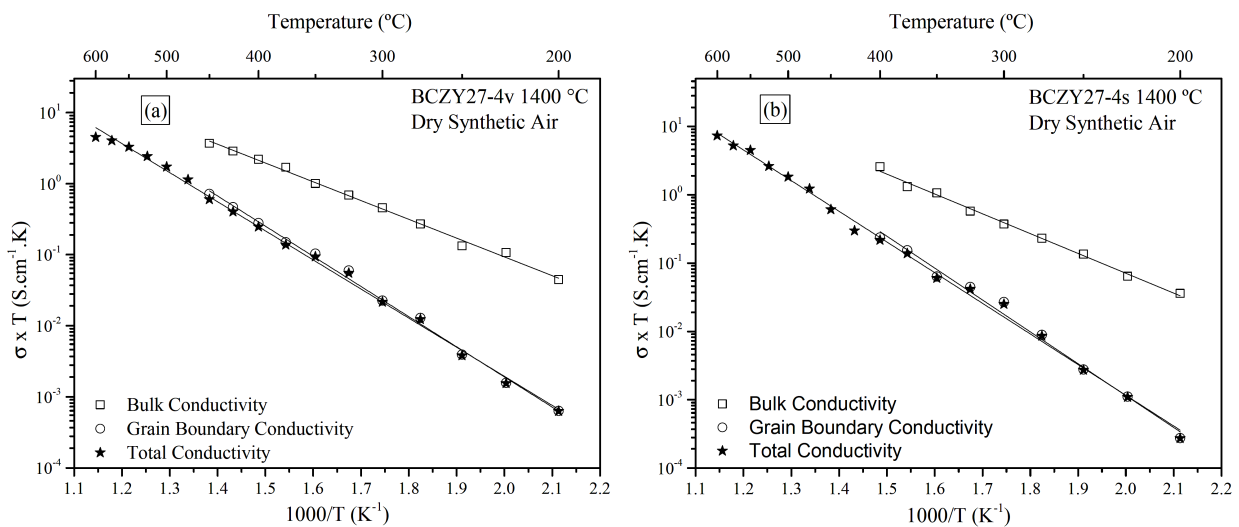


Figure 10. The Arrhenius plots of the bulk, grain boundary and total conductivity in dry air: a) BCZY27-4v and b) BCZY27-4s sintered at 1400 °C in synthetic air

the Arrhenius equation (Eq. 3) is lower for the bulk than for the grain boundary. The bulk activation energies found for the samples BCZY27-4s and BCZY27-4v are 0.47 eV and 0.49 eV, respectively. Both values are close to 0.5 eV, which is associated to the proton migration motion according to the Grotthuss mechanism [34–36]. Since these measurements were carried out in dry synthetic air, it can be presumed that the samples were partially hydrated. The grain boundary activation energies are 0.78 eV and 0.72 eV. The increase in activation energy values for grain boundaries indicates the existence of glassy layer of eutectic which hinders the proton transfer and thus reducing grain boundary conductivity [23].

Table 4. Activation energy values for the bulk (b), grain boundary (gb) and total (T) conductivity for BCZY27-4v and BCZY27-4s sintered at 1400 °C for 4 h

Sample	$E_a - b$ [eV]	$E_a - gb$ [eV]	$E_a - T$ [eV]
BCZY27-4v	0.49	0.78	0.74
BCZY27-4s	0.47	0.72	0.74

High energy milling processes might result in contaminations. However, the results of electrical measurements showed that even when using a high energy milling process, the electrical properties of the grain and the grain boundary were not diminished.

IV. Conclusions

The effectiveness of the milling process and addition of sintering aids was demonstrated with the produced $BaCe_{0.2}Zr_{0.7}Y_{0.1}O_{3-\delta}$ samples having densities higher than 90% TD at sintering temperature of 1300 °C. The samples produced with the BCZY27 powders without grinding and without sintering aids have small overall shrinkage. The density results showed that the BCZY27 powder grinding did not favour the densification of the samples even when sintered at 1600 °C for 12 h. The samples submitted to grinding in an eccentric mill with ZnO addition have an abrupt shrinkage increase indicating the liquid phase formation.

XRD analyses confirmed that the samples sintered at 1300 °C, in addition to the BCZY27 phase, contain small quantities of $BaCO_3$ and ZnO phases. In the samples sintered at 1400 °C, beside BCZY27 phase, a small amount of $Y_{0.4}Ce_{0.6}O_{1.8}$ was formed. With the increase in sintering temperature, the reaction between remaining $BaCO_3$ and ZnO phases leads to the $BaZnO_2$ formation.

Conductivity measurements in dry and wet synthetic air revealed no significant variation either in bulk, grain boundary and total conductivity as a function of the type of used milling process. The bulk activation energy was ~0.5 eV, corresponding to the proton conduction. The activation energy of the grain boundary was ~0.75 eV. This increase in activation energy value can be attributed to the presence of the glassy phase resulting from liquid phase formed during the sintering. The

total conductivity achieved at 500 °C (7.60×10^{-3} S/cm) is similar to the literature data.

Acknowledgements: The authors gratefully acknowledge the financial support from the Brazilian research funding agency CAPES - Brazil (National Council for the Improvement of Higher Education, processes No. 88881.030418/2013-01), CNPq - Brazil (National Council for Scientific and Technological Development, process No. 307128/2016-4).

References

1. Y. Zhang, H. Yhao, Z. Du, K. Świerczek, Y. Li, "High-performance $SbBaMn_2O_{5+\delta}$ electrode for symmetrical solid oxide fuel cell", *Chem. Mater.*, **31** (2019) 3784–3793.
2. P. Coddet, H. Liao, C. Coddet, "A review on high power SOFC electrolyte layer manufacturing using thermal spray and physical vapour deposition technologies", *Adv. Manuf. Fact.*, **2** (2014) 212–221.
3. N.Q. Minh, "Ceramic fuel cells", *J. Am. Ceram. Soc.*, **76** [3] (1993) 563–88.
4. A. Kirubakaran, S. Jain, R.K. Nema, "A review on fuel cell technologies and power electronic interface", *Renew. Sust. Energ. Rev.*, **13** [9] (2009) 2430–2440.
5. W. Sun, Z. Tao, Z. Shi, L. Yan, Z. Zhu, W. Liu, "Fabrication of $BaZr_{0.1}Ce_{0.7}Y_{0.2}O_{3-\delta}$ -based proton-conducting solid oxide fuel cells co-fired at 1,150 °C", *Fuel Cells*, **6** (2010) 1108–1113.
6. N.L.R.M. Rashid, A.A. Samat, A.A. Jais, M.R. Somalu, A. Muchtar, N.A. Baharuddin, W.N.R.W. Isahak, "Review on zirconate-cerate-based electrolytes for proton-conducting solid oxide fuel cell", *Ceram. Int.*, **45** [6] (2019) 6605–6615.
7. S. Ricote, N. Bonanos, M.C. Marco-de Lucas, G. Caboche, "Structural and conductivity study of the proton conductor $BaCe_{(0.9-x)}Zr_xY_{0.1}O_{(3-\delta)}$ at intermediate temperatures", *J. Power Sources*, **193** [1] (2009) 189–193.
8. L. Klein, M. Aparicio, A. Jitianu, *Handbook of Sol-Gel Science and Technology*, Second Edition, Springer International Publishing, 2018.
9. J. Wang, X. Chen, S. Xie, L. Chen, Y. Wang, J. Meng, D. Zhou, "Bismuth tungstate/neodymium-doped ceria composite electrolyte for intermediate-temperature solid oxide fuel cell: Sintering aid and composite effect", *J. Power Sources*, **428** (2019) 105–114.
10. P. Babilo, S.M. Haile, "Enhanced sintering of yttrium-doped barium zirconate by addition of ZnO", *J. Am. Ceram. Soc.*, **88** [9] (2005) 2362–2368.
11. M. Amsif, D. Marrero-López, J.C. Ruiz-Morales, S.N. Savvin, P. Núñez, "The effect of Zn addition on the structure and transport properties of $BaCe_{0.9-x}Zr_xY_{0.1}O_{3-\delta}$ ", *J. Eur. Ceram. Soc.*, **34** [6] (2014) 1553–1562.
12. C. Peng, J. Melnik, J.-L. Luo, A.R. Sanger, K. Chuang, "BaZr_{0.8}Y_{0.2}O_{3-δ} electrolyte with and without ZnO sintering aid: Preparation and characterization", *Solid State Ionics*, **181** [29–30] (2010) 1372–1377.
13. E.C. Grzebielucka, A.S.A. Chinelatto, S.M. Tebcherani, A.L. Chinelatto, "Synthesis and sintering of Y₂O₃-doped ZrO₂ powders using two Pechini-type gel routes", *Ceram. Int.*, **36** [5] (2010) 1737–1742.
14. S. Tao, J.T.S. Irvine, "Conductivity studies of dense yttrium-doped BaZrO₃ sintered at 1325 °C", *J. Solid State*

- Chem.*, **180** [12] (2007) 3493–3503.
15. G.S. Reddy, R. Bauri, “A novel route to enhance the sinterability and its effect on microstructure, conductivity and chemical stability of $\text{BaCe}_{0.4}\text{Zr}_{0.4}\text{Y}_{0.2}\text{O}_{3-\delta}$ proton conductors”, *Mater. Chem. Phys.*, **216** (2018) 250–259.
 16. N. Nasani, P.A.N. Dias, J.A. Saraiva, D.P. Fagg, “Synthesis and conductivity of $\text{Ba}(\text{Ce},\text{Zr},\text{Y})\text{O}_{3-\delta}$ electrolytes for PCFCs by new nitrate-free combustion method”, *Int. J. Hydrogen Energy*, **38** [20] (2013) 8461–8470.
 17. M. Hakim, J.H. Joo, C.-Y. Yoo, B.-K. Kim, J.H. Yu, “Enhanced chemical stability and sinterability of refined proton-conducting perovskite: Case study of $\text{BaCe}_{0.5}\text{Zr}_{0.3}\text{Y}_{0.2}\text{O}_{3-\delta}$ ”, *J. Eur. Ceram. Soc.*, **35** [6] (2015) 1855–1863.
 18. L.P. Wendler, K. Ramos, D.M.P.F. Souza, “Investigation about the reason of limited grain growth of Y-doped barium zirconate”, *Ceram. Int.*, **45** [15] (2019) 19120–19126.
 19. Z. Peng, R. Guo, Z. Yin, J. Li., “Influences of ZnO on the properties of $\text{SrZr}_{0.9}\text{Y}_{0.1}\text{O}_{2.95}$ protonic conductor”, *J. Am. Ceram. Soc.*, **91** [5] (2008) 1534–1538.
 20. Y. Li, Y. Guo, R. Ran, Z. Shao, “A novel approach for substantially improving the sinterability of $\text{BaZr}_{0.4}\text{Ce}_{0.4}\text{Y}_{0.2}\text{O}_{3-\delta}$ electrolyte for fuel cells by impregnating the green membrane with zinc nitrate as a sintering aid”, *J. Membrane Sci.*, **437** (2013) 189–195.
 21. Y. Li, R. Guo, C. Wang, Y. Liu, Z. Shao, J. An, C. Liu, “Stable and easily sintered $\text{BaCe}_{0.5}\text{Zr}_{0.3}\text{Y}_{0.2}\text{O}_{3-\delta}$ electrolytes using ZnO and Na_2CO_3 additives for protonic oxide fuel cells”, *Electrochim. Acta*, **95** (2013) 95–101.
 22. K. Uematsu, A. Terada, T. Morimoto, N. Uchida, K. Saito, “Direct determination of grain growth behavior in zinc oxide with added barium oxide”, *J. Am. Ceram. Soc.*, **72** [6] (1989) 1070–1072.
 23. H. Wang, R. Peng, X. Wu, J. Hu, C. Xia, “Sintering behavior and conductivity study of yttrium-doped BaCeO_3 - BaZrO_3 solid solutions using ZnO additives”, *J. Am. Ceram. Soc.*, **92** [11] (2009) 2623–2629.
 24. B.J.T.S. Irvine, D.C. Sinclair, A.R. West, “Electroceramics: Characterization by impedance spectroscopy”, *Adv. Mater.*, **2** [3] (1990) 132–138.
 25. T. Norby, “Solid-state protonic conductors: Principles, properties, progress and prospects”, *Solid State Ionics*, **125** [1-4] (1999) 1–11.
 26. K.D. Kreuer, “Proton-conducting oxides”, *Annu. Rev. Mater. Res.*, **33** [1] (2003) 333–359.
 27. K.D. Kreuer, “Aspects of the formation and mobility of protonic charge carriers and the stability of perovskite-type oxides”, *Solid State Ionics*, **125** [1] (1999) 285–302.
 28. D.Y. Wang, D.S. Park, J. Griffith, A.S. Nowick, “Oxygen-ion conductivity and defect interactions in yttria-doped ceria”, *Solid State Ionics*, **2** (1981) 95–105.
 29. J. Jiao, Q. Li, Y. Gu, Y. Luo, L. Ge, Y. Zheng, H. Chen, L. Gou, “Effect of $\text{BaO-B}_2\text{O}_3$ composite sintering aid on sinterability and electrical property of $\text{BaZr}_{0.85}\text{Y}_{0.15}\text{O}_{3-\delta}$ ceramic”, *Ceram. Int.*, **45** [11] (2019) 13679–13684.
 30. A.K. Baral, “Reduction in sintering temperature of stable proton conductor $\text{BaCe}_{0.35}\text{Zr}_{0.5}\text{Y}_{0.15}\text{O}_{3-\delta}$ prepared by sol-gel method and its transport properties”, *Solid State Ionics*, **272** (2015) 107–111.
 31. S. Barison, M. Battagliarin, T. Cavallin, L. Doubova, M. Fabrizio, C. Mortalo, S. Boldrini, L. Malavasi, R. Gerbasi, “High conductivity and chemical stability of $\text{BaCe}_{1-x-y}\text{Zr}_x\text{Y}_y\text{O}_{3-\delta}$ proton conductors prepared by sol-gel method”, *J. Chem. A*, **18** [42] (2008) 5120–5128.
 32. N. Nassani, Z. Shakel, F.J.A. Loureiro, B.B. Panigrahi, B.B. Kale, D.P. Fagg, “Exploring the impact of sintering additives on the densification and conductivity of $\text{BaCe}_{0.3}\text{Zr}_{0.55}\text{Y}_{0.15}\text{O}_{3-\delta}$ electrolyte for protonic ceramic fuel cells”, *J. Alloys Compd.*, **862** (2021) 158640.
 33. S. Ricote, N. Bonanos, G. Caboche, “Water vapour solubility and conductivity study of the proton conductor $\text{BaCe}_{(0.9-x)}\text{Zr}_x\text{Y}_{0.1}\text{O}_{(3-\delta)}$ ”, *Solid State Ionics*, **180** [14-16] (2009) 990–997.
 34. K.D. Kreuer, “On the complexity of proton conduction phenomena”, *Solid State Ionics*, **136-137** (2000) 149–160.
 35. N. Kochetova, I. Animitsa, D. Medvedev, A. Demin, P. Tsiakaras, “Recent activity in the development of proton-conducting oxides for high-temperature applications”, *RSC Adv.*, **6** [77] (2016) 73222–73268.
 36. E. Fabbri, D. Pergolesi, E. Traversa, “Materials challenges toward proton-conducting oxide fuel cells: A critical review”, *Chem. Soc. Rev.*, **39** [11] (2010) 4355–4369.